Spectrochimica Acta Part A: Molecular and Biomolecular Spectroscopy 137 (2015) 227–235

Contents lists available at ScienceDirect

Spectrochimica Acta Part A: Molecular and Biomolecular Spectroscopy

journal homepage: www.elsevier.com/locate/saa

Novel porphyrin–daunomycin hybrids: Synthesis and preferential binding to G-quadruplexes over i-motif

Ping Zhao [a,*], Shu-fang Jin [a], Jia-Zheng Lu [b,*], Jun-liang Lv [a], Gong-qing Wu [a], Pan-Pan Chen [a], Cai-Lian Tan [a], Dian-Wen Chen [a]

[a] School of Chemistry and Chemical Engineering, Guangdong Pharmaceutical University, No. 13, Changmingshui Road, Zhongshan 528458, PR China
[b] School of Pharmacy, Guangdong Pharmaceutical University, No. 280, Waihuandong Road, Education Mega Centre, Guangzhou 510006, PR China

HIGHLIGHTS

- Cationic porphyrin was firstly linked to a clinic drug, daunomycin.
- The porphyrin–daunomycin hybrids bind preferentially to G4 over i-motif DNA.
- Long-linked hybrids are more favorable in binding with G4 or i-motif structures.

GRAPHICAL ABSTRACT

The newly synthesized porphyrin–daunomycin hybrids could serve as prominent molecules to recognize guanine-rich (G4) and cytosine-rich (i-motif) DNA strands, with bis-intercalation to G4 (a) and non-specific binding to i-motif DNA (b).

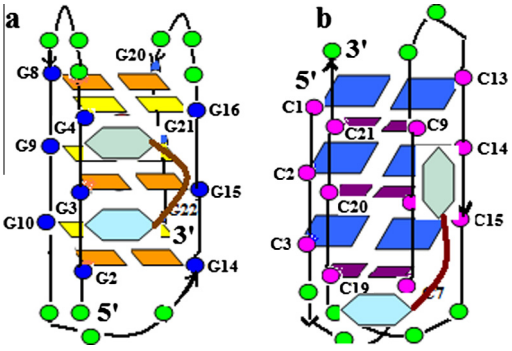

ARTICLE INFO

Article history:
Received 25 May 2014
Received in revised form 18 August 2014
Accepted 24 August 2014
Available online 4 September 2014

Keywords:
Porphyrin–daunomycin hybrids
G-quadruplexes
i-Motif

ABSTRACT

Encouraged by the enormous importance attributed to the structure and function of human telomeric DNA, herein we focused our attention on the interaction of a serious of newly prepared porphyrin–daunomycin (Por–DNR) hybrids with the guanine-rich single-strand oligomer (G4) and the complementary cytosine-rich strand (i-motif). Various spectral methods such as absorption and fluorescence titration, surface-enhanced Raman and circular dichroism spectrum were integrated in the experiment and it was found that these Por–DNR hybrids could serve as prominent molecules to recognize G4 and i-motif. What is more, interesting results were obtained that the hybrids with longer flexible links are more favorable in binding with both G4 and i-motif than the hybrid with shorter linkage. These Por–DNR hybrids may help to develop new ideas in the research of human telomeric DNA with small molecules.

Introduction

Telomeres are specific nucleoprotein structures and the telomeric DNA has a unique mode of replication based on a special reverse transcriptase enzyme called telomerase. By catalysing the synthesis of telomeric DNA, telomerase could maintain telomeric

* Corresponding authors. Tel./fax: +86 760 88207939 (P. Zhao). Tel./fax: +86 20 39352021 (J.-Z. Lu).
E-mail addresses: zhaoping666@163.com (P. Zhao), lujia6812@163.com (J.-Z. Lu).

http://dx.doi.org/10.1016/j.saa.2014.08.123
1386-1425/

DNA integrity and prevent critical telomere shortening with successive cell division so that cells cannot reach crisis points of senescence and apoptosis. Thus, telomerase play a critical role in cellular aging and cancer since they are essential for chromosomal stability and genome integrity [1,2]. Telomerase is up-regulated in 80–85% of tumor cells in comparison to normal somatic cells and is a major factor in cancer cell immortalisation. This unique activity of telomerase makes the enzyme an ideal probe for tumor diagnosis and a target for cancer chemotherapy. Therefore, currently there is considerable interest in finding molecules that can inhibit telomerase and potentially act as anti-cancer drugs [3–5].

Formation of a quadruplex DNA structure, which is incompatible with telomerase attachment to the 3′ end, is a promising approach to inhibit the enzyme. Human telomeric DNA consists of multiple repeated 5′-TTAGGG sequence on one strand and repeated 5′-CCCTAA sequence on the other one. However, the telomeric 3′-terminal DNA is composed of a single-stranded G-rich TTAGGG repeated overhang (approximately 100–200 bases) that can form G-quadruplex (G4) DNA structures in vitro [6–10]. Similarly, the complementary C-rich strand may also self-associate at pH 5.5 (a value close to the pK_a for free cytosine) into an intercalated structure called the i-motif based on intercalated C—C^+ base pairs [11,12] (Fig. 1). It is reported that quadruplex-binding and quadruplex-promoting small molecules can in principle effectively inhibit both the catalytic and capping functions of telomerase. Many small aromatic ligands, including porphyrins, quinacridones, anthraquinones, phenanthrolines, substituted triazines and acridines, have been shown to bind and stabilize the quadruplex structure of G-quadruplex DNA [13–15].

Porphyrins with their large aromatic structure and the four meso-positions available for substitution are interesting scaffold for the targeting of G-quadruplex DNA. In particular, the free base porphyrin (5,10,15,20-tetrakis(1-methyl-4-pyridyl)-21H,23H-porphine) (TMPyP4) has been intensively researched as a good G-quadruplex-binding model because of its unique symmetric structure and high positive charge [16,17]. On the other hand, daunomycin (DNR) is routinely used in the clinic for the treatment of leukemia, ovarian and breast carcinoma. In the past years, numerous anthracyclines derivatives have been synthesized with the aim of finding related compounds showing better DNA binding, which is closely related to higher therapeutic efficacy [18–20].

However, it is worth pointing out that the efforts on the research of DNR interactions with G-quadruplex and i-motif DNA are still inadequate in contrast to its considerable use as duplex DNA binders. Herein, we attached the clinic DNR molecules to cationic porphyrin through different flexible carbochains and tested their interactions with both G-quadruplex and i-motif DNA through the combination of various spectral methods. Since both the cationic porphyrin and DNR structures have positive charges and large molecular planes, it is expected that the integration of these two structures will be much favorable in DNA binding. Since it is well known that the structure of G-quadruplex DNA is cationic-sensitive (antiparallel in the presence of Na^+ and parallel in K^+ solution) while the i-motif is pH-sensitive (stable at a maximum pH value at 5.5) [6–12,21,22], all the experiments in this study were carried out in buffer A.

Experimental

Materials

Daunorubicin hydrochloride (Sigma), 1,3-dibromopropane, hexamethylene dibromide and 1,9-dibromononane (Sigma), silica gel (Qingdao) and chloroform (Guangzhou) were commercially

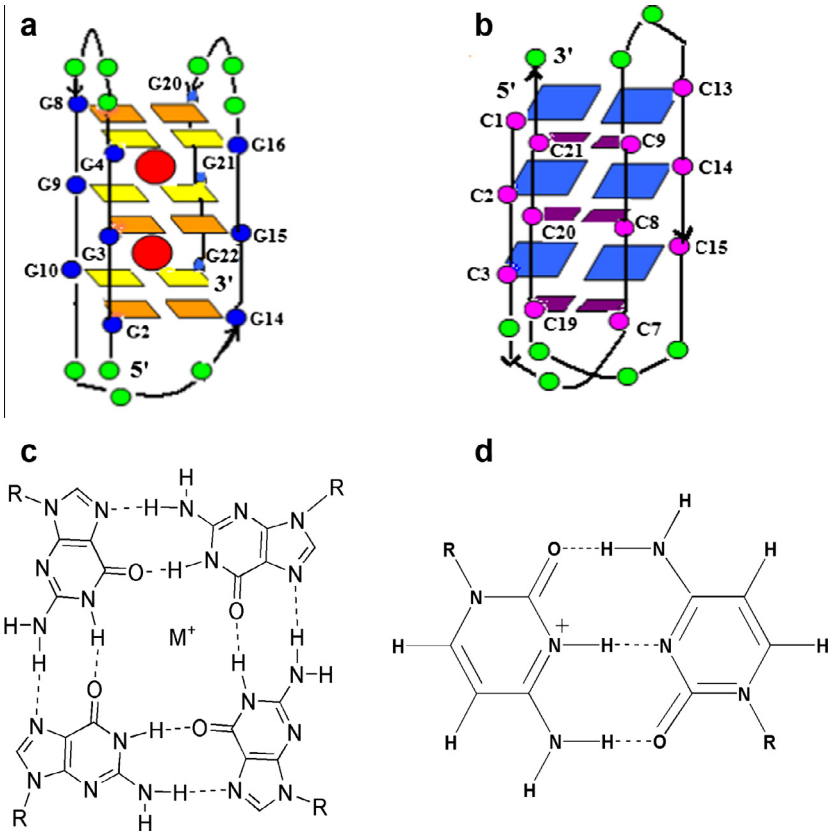

Fig. 1. Structures of a G-quartet showing the anti-parallel G-quadruplex topology in the sodium solution (a), i-motif (b), Hoogstaeen base pairing (c), C^+—C base pair (d) and of human telomeric sequences $AG_3(T_2AG_3)_3$ and $C_3(TA_2C_3)_3$. Arrows denoted 5′ → 3′ strand alignment for each DNA.

available and of analytical grade. MilliQ water was used to prepare buffer solutions. Buffer A (10 mM Tris–HCl, 1 mM EDTA and 100 mM NaCl, pH 5.5) solution was used in spectral, SERS and EB competing experiments and buffer B (10 mM Na_2HPO_4/NaH_2PO_4, 100 mM NaCl and 1 mM Na_2EDTA, pH 5.5) was used for thermal denaturation studies.

DNA oligomers 5′-AGGGTTAGGGTTAGGGTTAGGG-3′ (22 AG) and its corresponding complementary strand 5′-CCCTAACCC-TAACCCTAACCCT-3′ (22 CT) were purchased from Shanghai Sangon Biological Engineering Technology & Services Co., Ltd. (China) and used without further purification. The formations of intramolecular G4 and i-motif were carried out as follows: the oligonucleotide samples were dissolved in buffer A and heated to 90 °C for 5 min. Then the samples were gently cooled to room temperature, and incubated at 4 °C overnight. Concentrations of these oligomers were determined by measuring the absorbance at 260 nm after melting. Single-strand extinction coefficients were calculated from mononucleotide data using a nearest-neighbor approximation with the molar extinction coefficients at 260 nm are 215,000 and 185,900 M^{-1} cm^{-1} for 22 AG and 22 CT, respectively [23].

Instruments

Element analysis (C, H, and N) was carried out with a Perkin-Elmer 240 Q elemental analyzer. 1H NMR spectra were recorded on a Varian-300 spectrometer. All chemical shifts are given relative to tetramethylsilane (TMS). Electrospray Ionization mass spectra (ESI-MS) were recorded on a LCQ DECA XP system (Thremo, USA). UV–Vis spectra were recorded on a Hitech UV-3900 spectrophotometer. Fluorescence spectra were recorded on a Perkin-Elmer L55 spectrofluorophotometer. Circular dichroism (CD) spectra were recorded on a JASCO-J810 spectrometer. Surface-enhanced Raman spectroscopy (SERS) spectra were carried out on a Laser Micro-Raman Spectrometer of Renishaw in-via, with a power of 20 mW at the samples.

Methods

Absorption, fluorescence, CD spectrum

For absorption and fluorescence spectra, the aliquot DNA prepared in buffer A solution was added stepwise to the sample cell containing the Por–DNR hybrids. After equilibration for 10 min absorption or fluorescence spectrum were recorded. The titration processes were repeated until there was no change in the spectra for at least three titrations indicating the binding saturation had been achieved.

For CD spectra, Por–DNR hybrids mixed with G4 or i-motif DNAs at a ratio of [DNR]/[DNA] = 5 in the buffer A. The mixture was incubated at 4 °C overnight. Each measurement was the average of three repeated scans recorded with a 0.1 mm quartz cell with reaction volume of 1 mL at 25 °C. A background CD spectrum of corresponding buffer solution was subtracted from the average scan for each sample. CD spectrum of the compound alone (5 μM) was also measured in the buffer solution. Final analysis of the data was carried out using Origin 7.5 (Origin Lab Corp.).

SERS experiment

Ag colloids were prepared by reducing $AgNO_3$ with EDTA according to the reported method [24]. The Ag colloid/hybrid (or Ag colloid/DNA) SERS active systems were prepared by mixing equal volume of the hybrids (or DNA) solution with the Ag colloid in buffer A buffer to obtain the desired hybrid or DNA concentrations. In the hybrid/DNA complex experiments, the solution of DNA was mixed with the Por–DNR hybrid solution at a DNA/hybrid ratio of 30:1, then an equal volume of the mixed solution was fully mixed with the Ag colloid, and the spectrum was immediately measured at room temperature. The final concentrations of hybrids and DNA in all of the SERS-active systems were 5 and 150 μM, respectively.

Synthesis of hybrids

Porphyrin derivates. 5-(1-Bromopropylhydroxylphenyl)-10,15,20-tris(4-pyridiniumyl)-porphyrin (BrPPTPyP). 5-(4-Hydroxyphenyl)-10,15,20-tris(4-*N*-pyridiniumyl)porphyrin (HTPyP, formerly prepared [25]) was dissolved in a mixture of N,N-dimethylformamide (DMF) 6 mL. Then, Na_2CO_3 (100 mg) and 1,3-dibromopropane (68.7 mg, 0.34 mmol) were added. The reaction mixture was stirred at room temperature for 20–28 h. The progress of the reaction was monitored by TLC. After the reaction was complete, the reaction mixture was diluted with $CHCl_3$ and poured into water. The organic layer was separated and washed with water until neutral pH, dried over anhydrous Na_2SO_4, and evaporated under diminished pressure. The purple powder was dissolved in methylene chloride and chromatographed on silica gel using methylene chloride and ethanol (35:1) as eluent, collecting the first band from the column as the objective BrPPTPyP (178 mg, 0.153 mmol, 61.5% yield). ESI-MS *m*/*z* 753.2 ([M−H]−, calcd for $C_{44}H_{32}BrN_7O$: 754.3).

5-(Bromohexylhydroxylphenyl)-10,15,20-tris(4-pyridiniumyl)-porphyrin (BrHPTPyP) and *5-(1-bromodecylhydroxylphenyl)-10,15,20-tris(4-pyridiniumyl)-porphyrin (BrDPTPyP)* were similarly prepared, replacing 1,3-dibromopropane by hexamethylene dibromide and 1,10-dibromononane, respectively.

BrHPTPyP. Yield: 63.2%. ESI-MS *m*/*z* 795.2 ([M−H]−, calcd for $C_{47}H_{38}BrN_7O$: 796.2).

BrDPTPyP. Yield: 68.6%. ESI-MS *m*/*z* 851.3 ([M−H]−, calcd for $C_{51}H_{46}BrN_7O$: 852.3).

Synthesis of Por–DNR hybrids. The synthetic scheme of Por–DNR hybrids is shown in Scheme 1.

Synthesis of hybrid **1**. Daunorubicin hydrochloride was firstly dissolved in double distilled water and 5% NaOH solution was added to adjust the pH to 10. The daunorubicin was then precipitated and extracted by dichloromethane. The organic phase was evaporated and the deprotonated daunorubicin was obtained after drying under vacuum. Deprotonated daunorubicin (0.5 mmol, 0.272 g) and anhydrous K_2CO_3 (0.7 g) in dry DMF (20 mL) were stirred for 2 h at room temperature. Then BrPPTPyP (0.5 mmol, 0.376 g) was added to the activated daunorubicin, and the mixture was then stirred for 36 h at room temperature. The progress of the reaction was monitored by TLC. The reaction mixture was then diluted by $CHCl_3$ and DMF was washed out by water. The extracted crude material was purified by chromatography. Evaporation of solvent afforded compound, 5-(1-bromopropyl)-10,15,20-tris(4-Npyridiniumyl)porphyrin, (**1a** in Scheme 1) as a purple powder (yield: 0.394 g, 65%). **1a** was methylated in 5 mL of DMF with methyl iodide (0.8 mL) for 3 h at room temperature. The solvent and methyl iodide were removed under vacuum. Subsequently, the residue was dissolved in a 1 M solution of hydrochloride in methanol and then precipitated with ethyl ether as hydrochloride salt, which was washed with ethyl ether until neutral pH and dried under vacuum. Compound **1** was thus obtained quantitatively. Yield: 0.384 g, 94%. (Found: C, 67.38; H, 6.13; N, 8.32%. Calc. for $C_{75}H_{73}I_3O_{11}N_8.4H_2O$: C, 67.51; H, 6.07; N, 8.40%). ESI-MS *m*/*z* 319.3 (M^{4+}, calcd for $C_{75}H_{73}O_{11}N_8$: 1262.4). 1H NMR (300 MHz, DMSO): chemical shift δ 9.37 (d, *J* = 5.9 Hz, 6H, 2, 6-pyridinium), 9.07 (d, *J* = 6.6 Hz, 6H, 3,5-pyridinium), 8.90 (s, 8H, β-pyrrole), 8.16 (s, 2H, Por-2, 6-phenyl), 8.06 (s, 1H, DNR-phenyl), 7.83 (s, 1H, DNR-phenyl), 7.45 (s, 2H, Por-3,5-phenyl), 7.38 (s, 1H, DNR-phenyl), 6.1 (s, 4H, OH), 5.92 (s, 2H, NH_2), 5.2 (s, H, DNR-cyclo-H), 4.79 (s, 1H, DNR-cyclo-H), 4.73 (s, 9H, N^+—CH_3), 4.21 (s, 1H, DNR-cyclo-H), 4.11 (s, 2H, —CH_2—O), 3.95 (s, 3H, —O—CH_3), 3.91

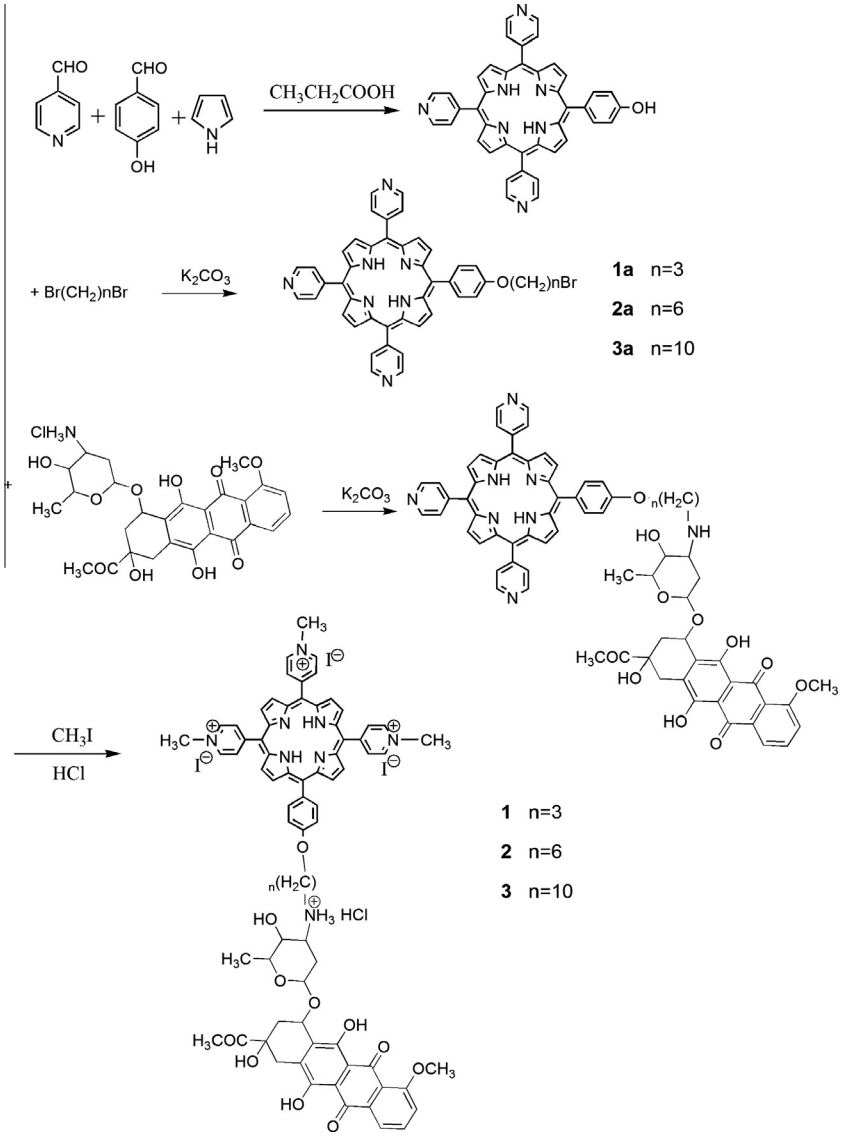

Scheme 1. The synthetic scheme of cationic Por–DNR hybrids.

(s, 1H, DNR-cyclo-H), 3.2 (s, 2H, CH_2—N), 3.11 (s, 1H, DNR-cyclo-H), 2.97 (d, *J* = 5.6 Hz, 2H, DNR-cyclo-H), 2.54 (s, 2H, —CH_2—), 2.41 (s, 3H, O═C—CH_3), 2.35 (d, *J* = 4.8 Hz, 2H, DNR-cyclo-H), 1.79 (s, 2H, DNR-cyclo-H), 1.06 (s, 3H, CH_3), −3.10 (s, 2H, NH pyrrole).

Compounds **2** and **3** were similarly prepared, replacing BrPPTPyP by BrHPTPyP and BrDPTPyP, respectively.

2, yield: 89%. (Found: C, 69.13; H, 6.22; N, 8.23%. Calc. for $C_{78}H_{78}I_3O_4N_8{\cdot}3H_2O$: C, 69.03; H, 6.19; N, 8.26%). ESI-MS *m*/*z* 330.3 (M^{4+}, calcd for $C_{78}H_{78}O_4N_8$: 1304.2). 1H NMR (300 MHz, DMSO): chemical shift δ: 9.38 (d, *J* = 5.9 Hz, 6H, 2, 6-pyridinium), 9.05 (d, *J* = 6.6 Hz, 6H, 3,5-pyridinium), 8.92 (s, 8H, β-pyrrole), 8.14 (s, 2H, Por-2, 6-phenyl), 8.04 (s, 1H, DNR-phenyl), 7.83 (s, 1H, DNR-phenyl), 7.4 (s, 2H, Por-3,5-phenyl), 7.37 (s, 1H, DNR-phenyl), 6.1 (s, 4H, OH), 5.92 (s, 2H, NH_2), 5.19 (s, H, DNR-cyclo-H), 4.8 (s, 1H, DNR-cyclo-H), 4.73 (s, 9H, N^+—CH_3), 4.21 (s, 1H, DNR-cyclo-H), 3.99 (s, 2H, —CH_2—O), 3.95 (s, 3H, —O—CH_3), 3.91 (s, 1H, DNR-cyclo-H), 3.2 (s, 2H, CH_2—N), 3.11 (s, 1H, DNR-cyclo-H), 2.97 (d, *J* = 5.6 Hz, 2H, DNR-cyclo-H), 2.41 (s, 3H, O═C—CH_3), 2.34 (d, *J* = 4.8 Hz, 2H, DNR-cyclo-H), 1.83 (d, *J* = 4.8 Hz, 4H, —$(CH_2)_2$—), 1.76 (s, 2H, DNR-cyclo-H), 1.26 (d, *J* = 4.8 Hz, 4H, —$(CH_2)_2$—), 1.04 (s, 3H, DNR-cyclo-CH_3), −2.95 (s, 2H, NH pyrrole).

3, yield: 87% (Found: C, 68.44; H, 6.65; N, 7.78%. Calc. for $C_{82}H_{86}I_3O_{11}N_8{\cdot}4.5H_2O$: C, 68.38; H, 6.61; N, 7.78%). ESI-MS *m*/*z* 344.1 (M^{4+}, calcd for $C_{82}H_{86}O_{11}N_8$: 1360.3).1H NMR (300 MHz, DMSO): chemical shift δ: 9.37 (d, *J* = 5.9 Hz, 6H, 2,6-pyridinium), 9.04 (d, *J* = 6.6 Hz, 6H, 3,5-pyridinium), 8.91 (s, 8H, β-pyrrole), 8.13 (s, 2H, Por-2, 6-phenyl), 8.06 (s, 1H, DNR-phenyl), 7.83 (s, 1H, DNR-phenyl), 7.4 (s, 2H, Por-3,5-phenyl), 7.35 (s, 1H, DNR-phenyl), 6.1 (s, 4H, OH), 6.01 (s, 2H, NH_2), 5.17 (s, H, DNR-cyclo-H), 4.8 (s, 1H, DNR-cyclo-H), 4.73 (s, 9H, N^+—CH_3), 4.2 (s, 1H, DNR-cyclo-H), 4.02 (s, 2H, —CH_2—O), 3.94 (s, 3H, s, 3H, —O—CH_3), 3.88 (s, 1H, DNR-cyclo-H), 3.11 (s, 1H, DNR-cyclo-H), 3.02 (s, 2H, CH_2—N), 2.97 (d, *J* = 5.6 Hz, 2H, DNR-cyclo-H), 2.4 (s, 3H, O═C—CH_3), 2.34 (d, *J* = 4.8 Hz, 2H, DNR-cyclo-H), 1.83 (d, *J* = 4.8 Hz, 4H, —$(CH_2)_2$—), 1.76 (s, 2H, DNR-cyclo-H), 1.54 (d, *J* = 4.8 Hz, 4H, —$(CH_2)_2$—), 1.26 (d, *J* = 5.6 Hz, 8H, —$(CH_2)_4$—), 1.04 (s, 3H, DNR-cyclo-CH_3), −2.94 (s, 2H, NH pyrrole).

Results and discussion

Synthesis

In our previous work, we have successfully obtained porphyrin–anthraquinone hybrids by attaching flexible carbochains to the anthraquinone molecules firstly and then linked to the porphyrin

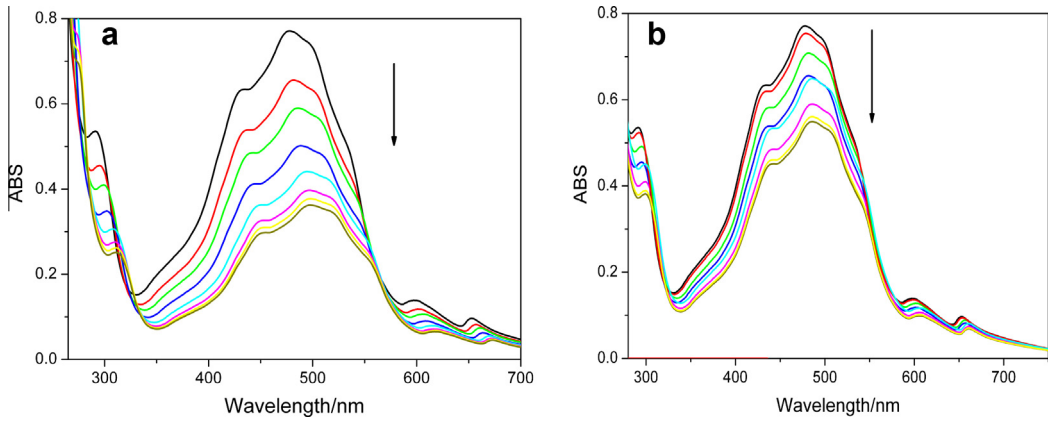

Fig. 2. Absorption spectra of **2** in buffer A at 25 °C in the presence of increasing amounts of 22 AG (a) or 22 CT (b). [DNR] = 10 μM. Arrows indicate the change in absorbance upon increasing the DNA concentration.

moiety [25]. However, this experience failed in synthesizing Por–DNR hybrids because the DNR molecule has more active groups than anthraquinone. Without the complex and troublesome group protection process, the active OH and NH_2 groups in DNR molecules will form rings when react with brominated carbon chains. Thus, we have to attach the flexible chains to the porphyrin part firstly rather than employ the synthetic scheme similar to porphyrin–anthraquinone hybrids. This method has the advantages of high productivity and effortlessness, with no group protection process needed.

DNA-binding properties

Absorption titrations

Fig. 2 exemplifies the absorption spectral changes of hybrid **2** upon G4-DNA and i-motif addition. With the increasing of G4-DNA (22 AG) and i-motif (22 CT) concentration, the absorption spectrum of the cationic Por–DNR hybrid **2** was significantly disturbed with hypochromism and bathochromism. This is an intuitional evidence of the compound–DNA binding behavior [26,27]. Similar spectral change was observed for hybrids **1** and **3**.

Table 1 summarizes the detailed titration data on G4-DNA and i-motif of all these three Por–DNR hybrids. From Table 1, all Por–DNR hybrids have larger hypochromism and red shift when binding with G4-DNA than with i-motif, suggesting that these hybrids have more intense interactions with the former. Meanwhile, hybrid **1** with shorter flexible linkages has smaller absorption change than **2** and **3**, from which we could consider that the Por and DNR moieties in hybrid **1** may suffer from steric hindrance and thus could not bind with the DNA structures flexibly. However, the longer bridging chain lengths in **2** and **3** decrease the steric hindrance between Por and DNR and the two moieties could employ more favorable binding modes.

Fluorescence titration studies

Fluorescence titration experiments of the hybrids in the presence of G4-DNA and i-motif were performed. When excited with 475 nm (hybrid's maximum excitation wavelength), the hybrids have similar emission spectra, ranging from 520 nm to 670 nm. In Fig. 3, fluorescence emission spectrum of **1** was selected to show the spectral change with increasing G4-DNA and i-motif and we can find that the fluorescence intensities were remarkably enhanced. Hybrids **2** and **3** have similar results and all these hybrids have smaller fluorescence change under i-motif than that under G4-DNA. Since the hydrophobic environment provided by DNA can protect the hybrid from quenching by water molecules, the emission increase is widely admitted as an indication of the interaction between compounds and DNA [28]. Thus, the different emission increase also suggests that the hybrids interact with G4-DNA more strongly than that with i-motif.

CD spectra

The CD spectral method, which is a very useful in distinguishing the DNA secondary structures, was employed to study the interaction of these hybrids with G4 and i-motif DNA. As shown in Fig. 4, none of these hybrids displays any CD spectral signal in the ultraviolet region. In the presence of Na^+, the CD spectrum of 22 AG shows a strong positive band at around 290 nm and a negative band at around 265 nm, which indicates the formation of an anti-parallel G-quadruplex structure [21]. Meanwhile, the CD spectra of C-rich strand alone showed a large positive band with a peak at 287 nm and a negative band centered at 255 nm, which is characteristic of the i-motif structure [22].

As to G4-DNA, in the presence of the hybrids **1**–**3**, the intensities of both positive and negative bands are increased significantly (Fig. 4a), which suggests that an anti-parallel structure is enhanced and stabilized by compounds [26]. However, excepted for slight red shifts in the positive peak and negative bands, no substantial changes were observed for i-motif in the presence of hybrids (Fig. 4b), implying that the hybrids affected the structure of i-motif to a certain extent [14,29,30]. The distinct CD spectral change between G4 and i-motif DNA indicates that the former may employ a more efficient binding with the hybrids than the latter. This

Table 1
Physical data of Por–DNR hybrids binding with G4 and i-motif DNAs.

Hybrid	UV–Vis spectra				ΔTm (°C)		K_b ($\times 10^6$ M^{-1})	
	G4		i-Motif		G4	i-Motif	G4	i-Motif
	Δλ (nm)	H%[a]	Δλ (nm)	H%				
1	10	31.47	5	22.31	4.1	5.8	8.3	4.4
2	17	53.04	8	27.32	14.2	6.7	9.2	5.8
3	16	51.35	7	32.78	9.3	4.2	8.5	5.1

[a] H% refers to the extent of hypochromism for absorption intensity.

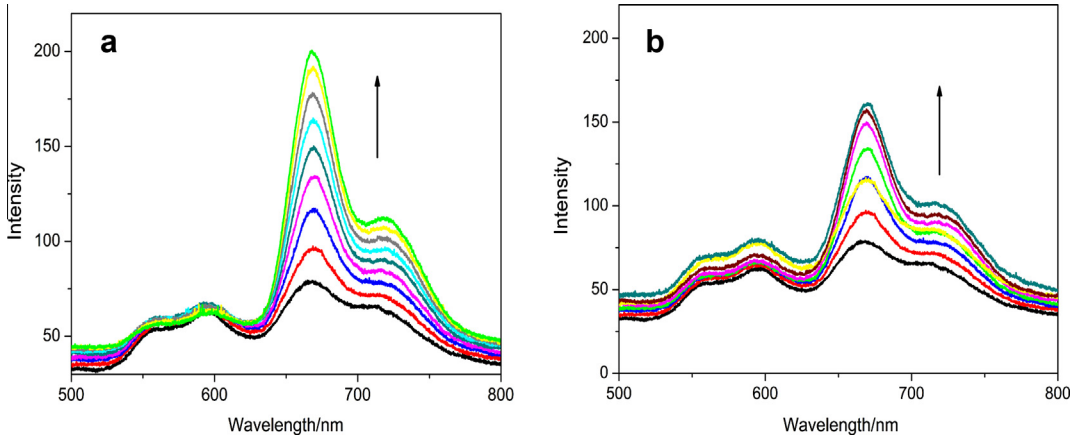

Fig. 3. Fluorescence emission spectra of **1** in buffer A upon increasing concentrations of 22 AG (a) or 22 CT (b). λ_{ex} = 475 nm. [DNR] = 10 μM. Arrows indicate the change in absorbance upon increasing the DNA concentration.

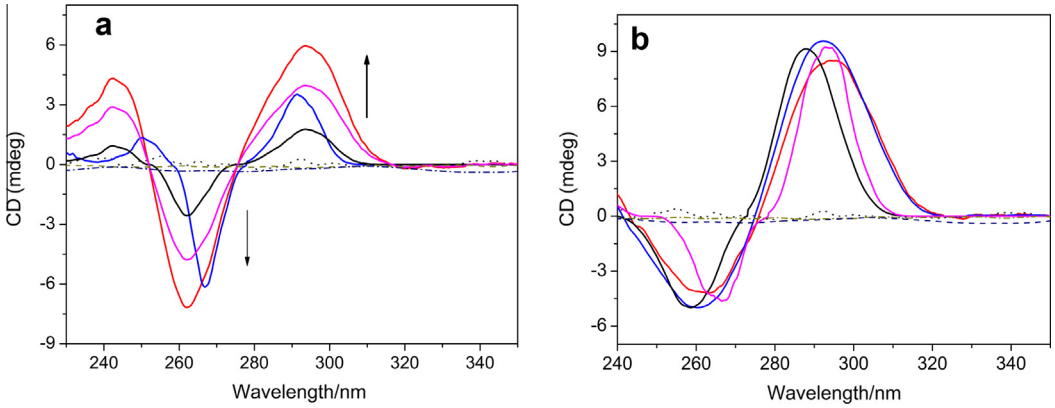

Fig. 4. CD spectra of free Por–DNR hybrids 1 (. . .), **2** (· –· –) and **3** (– – –), 22 AG (a) and 22 CT (b) in the absence (—) and in the presence of **1** (—), **2** (—) and **3** (—) in buffer A. [DNR]/[DNA] = 5. Arrows indicate the change in CD spectra upon increasing the concentration of the compounds.

result is in high consistent with the absorption and fluorescence titration experiments above.

SERS investigation

SERS is a powerful tool for the study of the interactions of compounds, especially fluorescence molecules, with biomacromolecules at very low concentrations. The silver colloids can be adapted for the application in the study of biological objects, because they do not modify to a great extent the structures of biological molecules adsorbed on their surface [24,31]. To further clarify the binding modes of these compounds to G4 DNA and i-motif, SERS spectra were measured.

The SERS spectra of free hybrid **1**, the Por–DNR hybrids in the presence of G4 and i-motif DNAs, are shown in Fig. 5. In the absence of DNA, free hybrids **1–3** show very similar SERS spectra because of their much similar molecular structures (see Fig. S1). Table 2 summarized the main SERS bands of the hybrids and their assignments. No substantial SERS signal is given by G4-DNA or i-motif, since the Ag colloids have negative charges on their surface, which repulses the adsorption of negative-charged DNA molecules [31–33].

The SERS intensities for all these hybrids in the presence of 22 AG were significantly decreased. In terms of the short-range character of the Raman enhancement in a colloid system, the SERS quenching is interpreted in term of a loss of accessibility for compounds to the Ag colloids [25,31–36]. The vanishment of bands centered at 330, 411, 814, 965, 1001, 1098, 1141 nm which are attributed to the porphyrin ring, indicating that the porphyrin structures of Ag-hybrid complexes were undetectable [25,31–36]. The result was suggested that, when binding with 22 AG, the porphyrin part of the hybrids may embed into the base pairs of G4-DNA structures, and thus was well protected by DNA molecules. Meanwhile, the band at 1545 cm^{-1} which is the characteristic band of anthraquinone plane significantly decreased [36],

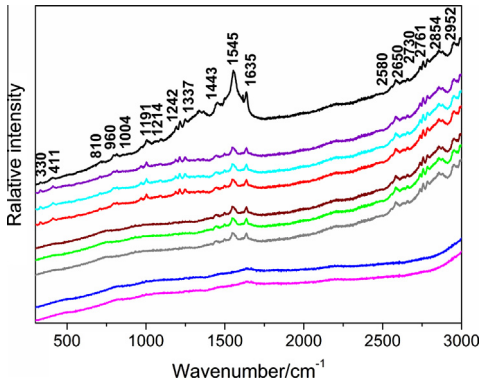

Fig. 5. SERS spectra (300–3000 cm^{-1}) of 22 AG (—), 22 CT (—), free hybrid 1 (—), 22 AG bound 1 (—), 2 (—), 3 (—) as well as 22 CT bound 1 (—), 2 (—), 3 (—). [DNA]/[DNR] = 30:1 in buffer A.

Table 2
Raman frequencies and assignments for Por–DNR hybrids.[a]

Raman shift (cm^{-1})	Assignments[b]	Raman shift (cm^{-1})	Assignments[b]
330	δ(por)	1337	ν_s(N—C_α)
411	δ(por) + ν(Ag—N)	1443	$\nu_s(CH_2)$
814	pyr ν(N^+—CH_3)	1500	$\nu_s(C_{14}—N_{15})$
	δ_s(por)	1554	ν(AQ)
965	ν(C_α—C_β)	1635	δ(pyr) + ν_s(C=O)
1001	ν(C_m—C_α)	2580	ν(C—H)
1098	δ_s(C_β—H)	2650	δ(cyclohexane)
1141	ν(C_α—N)	2730	ν(C—O_{12})
1191	δ(pyr), ν(N^+—CH_3)	2761	$\nu_s(CH_2)$
1214	δ(pyr), ν(C_α—N)	2854	ν(CH_3)
1242	ν(C_m—pyr)	2952	ν(CH_2)

[a] Band assignments are according to Refs. [25–34].
[b] *Abbreviations:* ν, stretching mode; δ, bending mode; s, symmetric mode; pyr, *N*-methylpyridinium; por, porphyrin core.

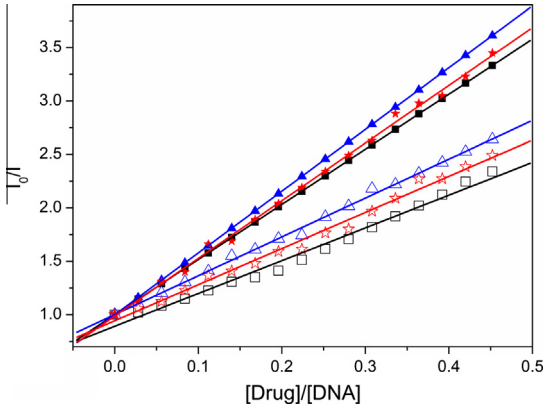

Fig. 6. Fluorescence quenching plots of 22 AG-bound EB in buffer A by **1** (▲), **2** (★) and **3** (■) in buffer A and 22 CT-bound EB by **1** (△), **2** (☆) and **3** (□) in buffer A. [DNA] = 100 μM, [EB] = 16.0 μM, λ_{ex} = 537 nm.

indicating that the anthraquinone moieties in DNR are also well protected by G4 DNA molecules. However, the remaining of bands ranging from 2500 to 3000 nm, which can be mainly ascribed to the sugar moieties in DNR and carbon links between porphyrin and DNR parts in the molecule [34–36], suggests that the sugar moieties and flexible carbon links may be still exposed in the solvent. These significant changes in the SERS intensities of the hybrids indicates that, the porphyrin and anthraquinone plane intercalate into G4-DNA bases because of their excellent planarity, while the sugar moieties and flexible carbon links bind on the surface or groove of the DNA structures. Namely, a "sandwich"-type interaction mode was employed here.

On the other hand, in the presence of i-motif, most of the characteristic porphyrin and DNR bands for these hybrids were still remained although the intensities significantly decreased, suggesting that the porphyrin and DNR moieties were still exists on the surface of the hybrid–DNA complexes rather than embedded in the i-motif molecules. The remained SERS signals indicate that the studied hybrids may bind to the i-motif molecules in a groove or end-pasting mode, which consists with the studies above.

Moreover, the chosen protocol for the SERS sample preparation allows the G4-hybrid adduct to be formed before its addition to the colloid solution (see Experimental). Consequently, the spectral changes confirm that the Por–DNR hybrid sufficiently bind to G4 DNA or i-motif even in Ag sols. In this medium, the preference of cationic hybrids for polyanionic G4-DNA or i-motif prevails over negatively charged Ag nanoparticles [37]. This result proves the tight binding affinities between the cationic hybrids and these DNA structures.

Competitive binding experiments with EB

For hybrids with multiple binding sites, traditional UV–Vis titration method is not suitable to determine K_b between hybrids and DNA [25,35]. Fluorescence spectrum was used to measure K_b by competition between EB and the studied hybrids for binding to DNA. This method measures the decrease of fluorescence of EB bound to DNA in the presence of the hybrid of interest. It can be used for all hybrids having a good affinity for DNA whatever their binding modes may be because it only measures the ability of a hybrid to compete with EB in binding with DNA [25,38,39].

The EB competitive binding experiments were carried out and quenching plots are given in Fig. 6. The quenching plots of I_0/I *vs* [DNR]/[DNA] are in good agreement with the linear Stern–Volmer equation. By taking K_b of 1.0×10^7 M^{-1} for EB with DNA, the K_b of these hybrids with G4 DNA and i-motif were calculated in Table 1 [25,38,39]. The binding affinities of the Por–DNR hybrids with 22 AG are larger than those with 22 CT, indicating that the G-quadruplex is a more favorable target compared with i-motif DNA. Meanwhile, the binding affinities of the Por–DNR hybrids with longer bridging links (**2** and **3**) are higher than that with shorter bridging link (**1**), in the both cases of G4 and i-motif DNAs. We suppose that both porphyrin and DNR moieties in the long-linked hybrids intercalate into DNA bases and both can replace EB from DNA helix, leading to relatively high binding affinities, whereas the short linked hybrids could not bis-intercalate DNA because of the steric hindrance.

Thermal denaturation studies

The melting curves of G4 DNA and i-motif in the absence and presence of hybrids are presented in Fig. 7. When mixed with the hybrids, the observed melting temperatures of G4-DNA and i-motif

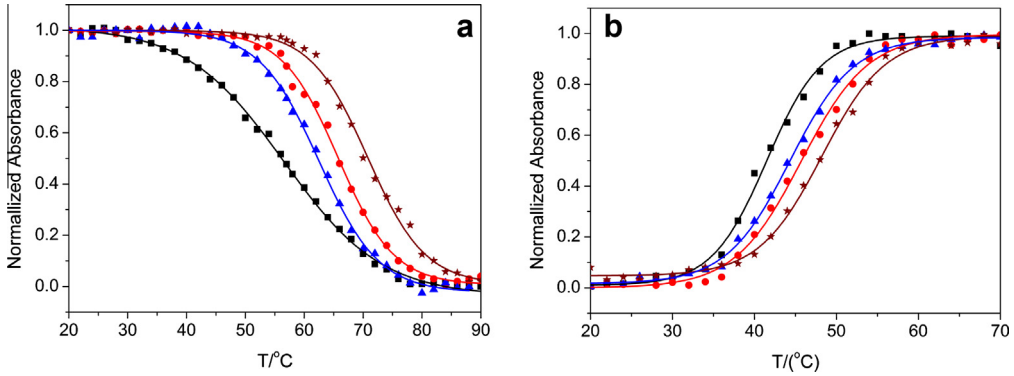

Fig. 7. Melting curves of 22 AG (a) and 22 CT (b) in the absence (■) and presence of **1** ▲), **2** (★) and **3** (●), in buffer B. [DNR] = 10 μM, [DNA] = 100 μM.

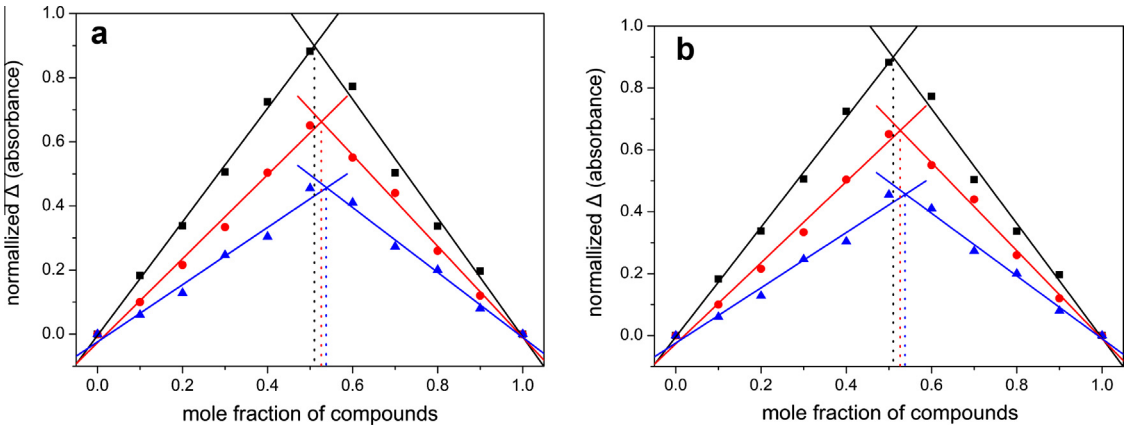

Fig. 8. Job plot resulting from the method of continuous variation analysis for hybrids **1** (▲), **2** (■) and **3** (●) with 22 AG (a) and 22 CT (b) in buffer A.

increase to different extents and the increases of Tm (ΔTm) are summarized in Table 1.

From Table 1, we can find that, in the presence of **1**, **2** and **3**, the values of ΔTm for 22 AG are relatively larger than those for 22 CT, suggesting that the hybrids have stronger DNA binding affinities with G4-DNA than with i-motif. [29,30]. This result is in consistent with the SERS spectra, from which we could observe smaller signal change of i-motif than G4-DNA. Meanwhile, the larger increases of **2** and **3** than **1** could be understood by the fact that the Por and DNR moieties in **2** and **3** could bind more flexibly while in **1** they suffer from steric hindrance. The results of thermal denaturation further argue for the DNA binding modes we mentioned above.

Continuous variation analysis

Continuous variation analysis (Job plot) was employed to determine the binding stoichiometry of hybrids with G4 and i-motif DNAs, as shown in Fig. 8. In the case of G4 DNA, the intersection points were 0.50, 0.54, and 0.55 for hybrids **1**, **2** and **3**, respectively, which corresponded to the stoichiometric ratio of 1:1 (one hybrid molecule to per quadruplex), whereas the corresponding values were 0.51, 0.53 and 0.53 for i-motif/hybrid, suggesting their binding stoichiometric ratios were also 1:1.

Ma et al. has reported a compound contained a pendant COOH functional group which was found to have a strong preference for binding to G-quadruplexes, which might be involved in H-bonding interaction with the guanine in the external tetrad of G-quadruplex DNA [40]. It is supposed that, besides the different binding modes, the preferential selectivity of the Por–DNR hybrids to G4-DNA than i-motif may also relate to the H-bonding interaction between the guanine in the external tetrad of G-quadruplex DNA and the OH groups in DNR moiety of the hybrids.

Conclusion

Herein the authors introduced a series of cationic Por–DNR hybrids with various bridging links and investigated their binding behaviors with 22 AG (G4 DNA) and 22 CT (i-motif DNA). Spectral, thermodynamic and hydrodynamic experiments indicate these Por–DNR hybrids are good selectors to G4 DNA than to i-motif, which may closely relate to the OH groups in DNR structure and the different steric hindrance between two moieties of the hybrids. Meanwhile, the hybrids with longer flexible links are more favorable in binding with both G4 and i-motif than the hybrid with shorter linkage. This indicated that modifying the structures of complexes could create some interesting differences in the DNA-binding properties, therefore, such structural information of the complexes was important for a more comprehensive understanding of the biological implications of these structures and for designing new compounds with enhanced activity and minimized undesired toxicity. Further efforts on the biological research such as cytotoxicity and cellular uptake are currently underway.

Acknowledgements

This work was financially supported by the National Nature Science Foundation of China (21101033) and Guangdong Pharmaceutical University.

Appendix A. Supplementary material

Supplementary data associated with this article can be found, in the online version, at http://dx.doi.org/10.1016/j.saa.2014.08.123.

References

[1] Y. Kawamoto, T. Bando, F. Kamada, Y. Li, K. Hashiya, K. Maeshima, H. Sugiyama, J. Am. Chem. Soc. 135 (2013) 16468–16477.
[2] S.E. Altschuler, T.H. Dickey, D.S. Wuttke, Biochemistry 50 (2011) 7503–7513.
[3] R. Rodriguez, S. Müller, J.A. Yeoman, C. Trentesaux, J.F. Riou, S. Balasubramanian, J. Am. Chem. Soc. 130 (2008) 15758–15759.
[4] H.R. Zhang, M.S. Wu, J.J. Xu, H.Y. Chen, Anal. Chem. 86 (2014) 3834–3840.
[5] H. Yaku, T. Murashima, D. Miyoshi, N. Sugimoto, J. Phys. Chem. B 118 (2014) 2605–2614.
[6] L.Q. Wang, Y. Zhang, C.Y. Zhang, Anal. Chem. 85 (2013) 11509–11517.
[7] A. Jain, A. Paul, B. Maji, K. Muniyappa, S. Bhattacharya, J. Med. Chem. 55 (2012) 2981–2993.
[8] C.Y. Chen, Q. Wang, J.Q. Liu, Y.H. Hao, Z. Tan, J. Am. Chem. Soc. 133 (2011) 15036–15044.
[9] S. Bhattacharya, P. Akash, K. Jain, A. Paul, Bioconjugate Chem. 21 (2010) 1148–1159.
[10] D. Piekna-Przybylska, M.A. Sullivan, G. Sharma, R.A. Bambara, Biochemistry 53 (2014) 2581–2593.
[11] J. Choi, S. Kim, T. Tachikawa, M. Fujitsuka, T. Majima, J. Am. Chem. Soc. 133 (2011) 16146–16153.
[12] J. Zhang, X. Wang, Y. Fu, Y. Han, J.Y. Cheng, Y.Q. Zhang, W. Li, Langmuir 29 (2013) 14345–14350.
[13] I.M. Dixon, F. Lopez, A.M. Tejera, J.P. Estève, M.A. Blasco, G. Pratviel, B. Meunier, J. Am. Chem. Soc. 129 (2007) 1502–1503.
[14] M. Schoonover, S.M. Kerwin, Front. Nucleic Acids 2 (2011) 13–32.
[15] S. Neidle, G. Parkinson, Nat. Rev. Drug Discov. 1 (2002) 383–393.
[16] G.N. Parkinson, R. Ghosh, S. Neidle, Biochemistry 46 (2007) 2390–2397.
[17] Y.P. Bhavsar-Jog, E.V. Dornshuld, T.A. Brooks, G.S. Tschumper, R.M. Wadkins, Biochemistry 53 (2014) 1586–1594.
[18] K.W. Lim, Z.J. Khong, A.T. Phan, Biochemistry 53 (2014) 247–257.
[19] C. Daniela, C. Alessandro, L. Giuseppina, C. Nicola, C. Maurizio, D.G. Gaia, R. Mara, V. Fabrizio, F. Cesare, M.C. Carlo, J. Am. Coll. Cardiol. 55 (2010) 213–220.
[20] J.H. Tan, Q.X. Zhang, Z.-S. Huang, Y. Chen, X.-D. Wang, L.Q. Gu, J.Y. Wu, Eur. J. Med. Chem. 41 (2006) 1041–1047.
[21] G.N. Parkinson, M.P. Lee, S. Neidle, Nature 417 (2002) 876–880.
[22] J.L. Mergny, L. Lacroix, X.G. Han, J.L. Leroy, C. Helene, J. Am. Chem. Soc. 117 (1995) 8887–8898.
[23] C.R. Cantor, M.M. Warshaw, H. Shapiro, Biopolymers 9 (1970) 1059–1077.

[24] J. Chen, J.M. Hu, Z.S. Xu, R.S. Sheng, Appl. Spectrosc. 47 (1993) 292–295.
[25] P. Zhao, L.C. Xu, J.W. Huang, B. Fu, H.C. Yu, L.N. Ji, Bioorg. Chem. 36 (2008) 278–287.
[26] L.H. Wang, Y. Wen, J. Liu, J. Zhou, C. Li, C.Y. Wei, Org. Biomol. Chem. 9 (2011) 2648–2653.
[27] P. Zhao, L.C. Xu, J.W. Huang, B. Fu, H.C. Yu, L.N. Ji, Biophys. Chem. 135 (2008) 102–109.
[28] L.N. Ji, X.H. Zou, J.G. Liu, Coord. Chem. Rev. 513 (2001) 216–217.
[29] L.H. Wang, Y.B. Wu, T.G. Chen, C.Y. Wei, Int. J. Biol. Macromol. 52 (2013) 1–8.
[30] S. Shi, X.T. Geng, J. Zhao, T.M. Yao, C.R. Wang, D.J. Yang, L.F. Zheng, L.N. Ji, Biochimie 92 (2010) 370–377.
[31] C.Y. Wei, G.Q. Jia, J.L. Yuan, Z.C. Feng, C. Li, Biochemistry 45 (2006) 6681–6691.
[32] J.D. Groot, R.E. Hester, J. Phys. Chem. 91 (1987) 1693–1696.
[33] M. Procházka, P.Y. Turpin, J. Stepánek, J. Bok, J. Mol. Struct. 482–483 (1999) 221–224.
[34] S.N. Terekhov, S.G. Kruglik, V.L. Malinovskii, V.A. Galievsky, V.S. Chirvony, P.Y. Turpin, J. Raman Spectrosc. 34 (2003) 868–881.
[35] E. Gaudry, J. Aubard, H. Amouri, G. Levi1, C. Cordier, Biopolymers 82 (2006) 399–404.
[36] Y.C. Ning, Structure Identification of Organic Compounds and Organic Spectroscopy, Science Press, Tsinghua, Beijing, 1991. pp. 485–498.
[37] E. Gaudry, J. Aubard, H. Amouri, G. Lévi1, C. Cordier, Biopolymers 82 (2006) 399–404.
[38] M.A. Sari, J.P. Battioni, D. Dupre, D. Mansuy, J.B. Lepecq, Biochemistry 29 (1990) 4205–4215.
[39] T. Jia, Z.X. Jiang, K. Wang, Z.Y. Li, Biophys. Chem. 119 (2006) 295–302.
[40] D.L. Ma, C.M. Che, S.C. Yan, J. Am. Chem. Soc. 131 (2009) 1835–1846.